How to cite: *Angew. Chem. Int. Ed.* **2021**, *60*, 24709–24715
International Edition: doi.org/10.1002/anie.202111620
German Edition: doi.org/10.1002/ange.202111620

Batteries

High-Performant All-Organic Aqueous Sodium-Ion Batteries Enabled by PTCDA Electrodes and a Hybrid Na/Mg Electrolyte

*Martin Karlsmo, Roza Bouchal, and Patrik Johansson**

Abstract: *Aqueous sodium-ion batteries (ASIBs) are aspiring candidates for low environmental impact energy storage, especially when using organic electrodes. In this respect, perylene-3,4,9,10-tetracarboxylic dianhydride (PTCDA) is a promising anode active material, but it suffers from extensive dissolution in conventional aqueous electrolytes. As a remedy, we here present a novel aqueous electrolyte, which inhibits the PTCDA dissolution and enables their use as all-organic ASIB anodes with high capacity retention and Coulombic efficiencies. Furthermore, the electrolyte is based on two, hence "hybrid", inexpensive and non-fluorinated Na/Mg-salts, it displays favourable physico-chemical properties and an electrochemical stability window >3 V without resorting to the extreme salt concentrations of water-in-salt electrolytes. Altogether, this paves the way for ASIBs with both relatively high energy densities, inexpensive total cell chemistries, long-term sustainability, and improved safety.*

Introduction

For renewably sourced energy, sustainable energy storage technologies are imperative to reach for example, the greenhouse gas (GHG) emission goals set by the UN by 2030.[1,2] Rechargeable batteries arguably offer the best combination of energy efficiency and versatility,[3,4] but the currently dominant technology, the lithium-ion battery (LIB), is connected with both high cost (while rapidly declining[5]) and resource issues; cobalt, and as the cobalt content decreases; nickel, as well as natural graphite and lithium itself. The LIBs also require a Cu current collector on the anode side, adding both cost and GHGs at the manufacturing stage.[6]

[*] M. Sc. M. Karlsmo, Dr. R. Bouchal, Prof. P. Johansson
Department of Physics
Chalmers University of Technology
41296 Göteborg (Sweden)
E-mail: patrik.johansson@chalmers.se
Prof. P. Johansson
ALISTORE-ERI, CNRS FR 3104
Hub de l'Energie
80039 Amiens Cedex (France)
Supporting information and the ORCID identification number(s) for the author(s) of this article can be found under: https://doi.org/10.1002/anie.202111620.

Sodium-ion batteries (SIBs) are an alternative technology void of most of these resource issues and offer both decreased cost, improved power performance, and have at least the prospect of similar gravimetric energy densities as compared to LIBs.[7–10] Furthermore, as Na does not alloy with Al, there is no need for any Cu current collectors. SIBs do in general have similar electrolyte and electrode layouts as LIBs; the former consist of a Na-salt dissolved in organic carbonate solvents, while the cathodes are transition metal oxides and the anode of choice is hard carbon (HC) (as opposed to graphite).[11] Especially the latter raises concerns of long-term sustainability if not derived from abundant biomaterial precursors.[12] One alternative SIB layout that alleviates many of these issues is all-organic batteries made entirely/mainly from renewable resources.[13] Indeed, many organic electrode active materials have been explored for SIBs, using both non-aqueous[6] and aqueous[14] electrolytes. So far many SIB electrodes fail to deliver their redox capacities with, or they detrimentally dissolve into, aqueous electrolytes.[15–17] If realised, however, an aqueous sodium-ion battery (ASIB) would bring low cost, eco-friendliness, high rate ability, improved safety, and be very suited for large-scale storage applications.[18] Thus, this is a most promising path to explore.

Starting from the aqueous electrolytes, they all suffer from rather narrow electrochemical stability windows (ESWs), which limits both the cell energy density and the applicable electrode materials. As of today, 1 M $Na_2SO_{4(aq)}$ is the most commonly used electrolyte for ASIBs with an ESW of ca. 2 V, a high ion conductivity (ca. 100 mS cm^{-1}), a low viscosity (ca. 1.2 mPa s), low inherent materials cost, high safety and compatibility towards many electrode materials.[18] The anodes have almost without exception been based on $NaTi_2(PO_4)_3$ as active material ever since its introduction in 2011.[19] Mainly due to its high capacity (120 mAh g^{-1}) and low electrochemical potential (−0.9 V vs. Ag/AgCl), it is still the state-of-the-art ASIB anode, while further advances have been relatively scarce.[20] However, its potential is below the reduction limit of most ASIB electrolytes and it also requires an oxygen-free environment to avoid oxidation.[21] As for organic alternatives, the biomolecule alizarin,[22] the non-faradaic capacitive activated carbon (AC),[23,24] and various polyimides[25,26] are as of today the only viable ASIB anodes. None of these, however, offers any appreciable capacity in combination with long-term stability at practical C-rates.

β-Perylene-3,4,9,10-tetracarboxylic dianhydride (β-PTCDA) was originally studied as an organic LIB cathode material,[27] but later α-PTCDA (henceforth PTCDA) was applied in SIBs and shown to reversibly intercalate two Na^+ ions.[28] β-PTCDA and α-PTCDA have slightly different crystal structures, but belong to the same space group and

display very similar characteristics.[29] PTCDA has also been used, now as anode, together with aqueous electrolytes to create potassium, hydronium and magnesium batteries, but suffers from extensive dissolution in conventional electrolytes.[17,30,31] For the former, a 30 m KFSI water-in-salt electrolyte (WISE) was applied, resulting in significantly improved capacity retention and also a broadened ESW.[17] While WISEs limit the dissolution of active material,[32,33] they are intrinsically based on high salt concentrations, of a salt which often is expensive and fluorinated, and hence defeats the aim of aqueous batteries to be low cost, safe, and environmentally benign.[34,35]

Herein, we demonstrate PTCDA in a half-cell as a high-performant anode for all-organic ASIBs. This is made possible by the use of an aqueous electrolyte based on two Na/Mg-salts (Na_2SO_4 and $MgSO_4$), hence the use of the notation "hybrid", both of which are inexpensive and non-fluorinated, at more intermediate salt concentrations. This should also render this electrolyte relatively low viscosity—important both for wetting of the electrodes and to avoid transport limitations at high current rates. As a side-note; in the very final stages of preparing this paper, we found such a type of hybrid electrolyte just being reported for ASIBs, but with all information except the Abstract exclusively available in Chinese.[36] We here start by investigating the fundamental physico-chemical properties of different Na_2SO_4-based electrolytes and our hybrid electrolyte, before we assess the ESWs and the local water structures, and finally we electrochemically characterise the PTCDA electrodes and their functionality in ASIBs.

Results and Discussion

First, the effects of electrolyte salt concentration on basic physico-chemical properties: densities, viscosities, and ion conductivities, are presented. From these data, a Walden analysis was made to determine the ionicities of the electrolytes as a measure of ion–ion dissociation. Thereafter, the ESWs are presented for the electrolytes in conjunction with a Raman spectroscopy analysis, to provide insight on the possible role of the local structure. Finally, we present the electrochemical characterisation of PTCDA in the various electrolytes, to elucidate possible ASIB performance promises, including post-mortem studies of the active material dissolution.

Electrolyte Physico-Chemical Properties

Starting with the densities of the electrolytes, these, as expected, increase more or less linearly as a function of salt concentration (Figure 1a), while the viscosities increase exponentially (Figure 1b), and both decrease as a function of temperature (Figure 1ab). The hybrid electrolyte (1.9 + 2.4 m) displays a viscosity of ca. 9 mPa s at 30 °C, which is half an order of magnitude higher than for the most concentrated Na_2SO_4 based electrolyte (ca. 1.9 mPa s at 30 °C). As compared to WISEs, however, the hybrid electrolyte is still very fluid; for example, a 35 m NaFSI WISE renders 97 mPa s,[37] and thus it is still of reassuringly low viscosity and this property should not severely limit the ASIB performance.

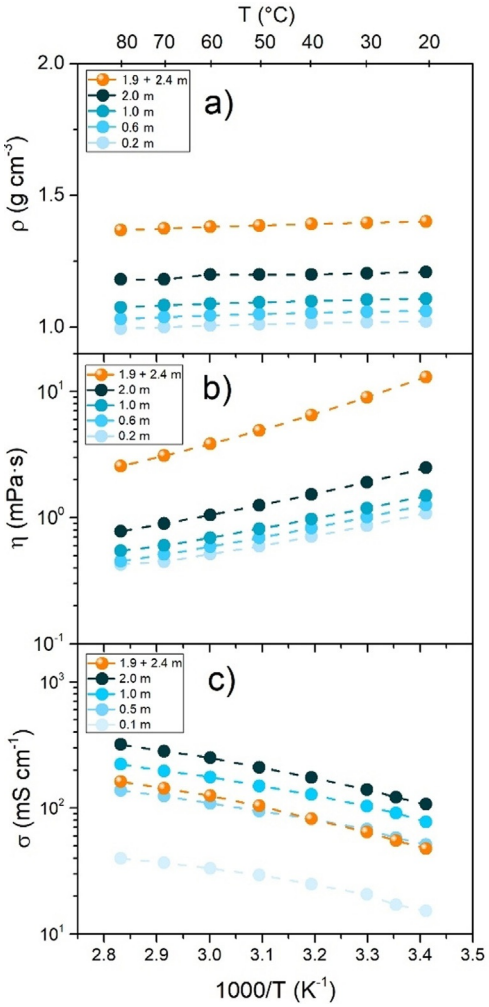

Figure 1. Arrhenius plots of the: a) density, b) viscosity, and c) ion conductivity for the Na_2SO_4-based aqueous electrolytes. Dashed lines to guide the eye only.

The intrinsic high ion conductivities of aqueous electrolytes are confirmed, continuously increasing, from 17 mS cm^{-1} at 0.1 m to 122 mS cm^{-1} at 2.0 m (Figure 1c). For the hybrid electrolyte, the ion conductivity decreases less than what would be expected based on the increased viscosity, relative to the same Na_2SO_4 concentration, to 55 mS cm^{-1} at 30 °C, pointing to some synergy. There is clearly an increase in the charge carrier concentration, but perhaps also somewhat different structure and dynamics as the temperature dependence differs (Figure 1c). Reassuring from a methodology point-of-view all the electrolytes have ion conductivities of the same order of magnitude as NaTFSI-, NaFSI-, and $NaClO_4$-based aqueous electrolytes.[38–40]

Continuing, a VFT analysis [Eq. (S1),(S2)][41,42] of the density (Figure S1a) and ion conductivity data (Figure S1b), shows the pseudo-activation energies (Table S1,S2) to increase as function of salt concentration, in accordance with

the literature.[37,43,44] Notably the hybrid electrolyte behaves similarly to the 0.5–1.0 m Na_2SO_4 electrolytes. We note that $T_{0\sigma}$ increased as function of salt concentration for aqueous KAc electrolytes, whereas LiFSI- and NaFSI-based electrolytes did not show any such behaviour,[37,43] as is the case for all our electrolytes. Similarly, our η_0 has no clear concentration correlation, whereas for the 1 to 25 m KAc electrolytes it spans over several orders of magnitude. Finally, our σ_0 parameter follows the pseudo-activation energy trend, in accordance with NaFSI electrolyte, in contrast to LiFSI electrolytes, and KAc electrolytes show an initial increase, but then remains constant for concentrations >5 m. As we have no comparable data where either cation or anion is the same as in our systems, any further analysis would be very speculative.

Finally, a Walden plot is made to decipher the relationship between the electrolytes' equivalent molar conductivities and viscosities,[45] and qualitatively visualise their ionicities and classify their ion conducting behaviour (Figure 2). All data points are close to the ideal KCl line and thus the ions fully dissociate (Figure 2). Furthermore, as the slopes are close to unity, the activation energies for ion conductivity and viscosity are similar, and hence the ion transport mechanism is very likely to be mainly vehicular,[46] in agreement with the VFT pseudo-activation energies (Tables S1,S2).

As we here use not only monovalent salts, there is a need for some elaboration on how to properly represent our data in a Walden plot. We start from Dave et al. who compared Na_2SO_4 and $NaNO_3$ electrolytes and claimed the (apparent) higher ionicity of the former to originate from the stoichiometry difference.[47] Moreover, the highly charged SO_4^{2-} could also make less solvent available for the cation, rendering smaller Na^+ first solvation shells. Indeed, if we here apply a scaling methodology and divide the molar conductivities by two (Na_2SO_4 $^1/_2\Lambda$), according to Equation (S3), the ionicities of our electrolytes become akin to aqueous NaTFSI and NaFSI electrolytes.[48,49] On the other hand, considering the molar conductivities at face value, all the electrolytes can be classified as slightly superionic, that is, the ionic conductivity and the viscosity are somewhat decoupled, thus the ions move faster than expected solely based on the viscosity.[50] Notably, the hybrid electrolyte data are positioned furthest away from the ideal line and thus display the highest ionicities.

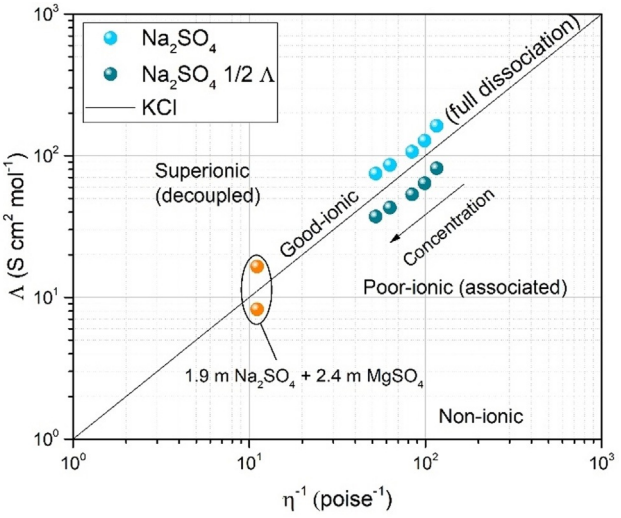

Figure 2. Walden plot of the aqueous electrolytes at 30 °C. The Na_2SO_4 $^1/_2\Lambda$ data use scaled molar conductivities (see text).

Electrolyte Electrochemical Stability and Local Structure

With increased electrolyte salt concentration the ESW expands, at both the oxidative and reductive limit, by 0.2 V from 3.5 to 3.7 V (Figure 3; at 1 mA cm^{-2}). In the literature, the ESW for 1 M Na_2SO_4 is 1.5–2.0 V using stainless steel as WE and a scan rate of 0.1 mV s^{-1},[51] and up to 2.2 V using Ti grids as WE at a scan rate of 5 mV s^{-1}.[52] Thus ours is much larger, but both the scan rate and the WE affect the ESW; Ti and glassy carbon tend to have large overpotentials, moving the water splitting reaction to higher voltages.[53] The current density limit at which the ESW is defined is also not set in stone, varying vastly among authors and is sometimes not communicated. Nevertheless, using our approach the hybrid electrolyte has a slightly wider ESW, 3.9 V (Figure 3b), now due to the oxidative limit moving to higher potentials. In addition, the small wave-like feature at ca. 1.25 V, observed for all the other electrolytes, is completely suppressed.

Whether this phenomenon is thermodynamic or also has a kinetic component—as the viscosity of the hybrid electrolyte is much higher—remains an open question.

Even if the exact magnitude may differ, it is clear from the above that there is substantial difference in the ESWs, and especially for the on-set of the oxidation. Arguably, this might originate in changes in the electrolyte local structure and/or dynamics. From the Raman spectroscopy analysis of the OH-stretching modes, we find a shifted and a narrowed overall broad band envelope as function of salt concentration, including the hybrid electrolyte (Figure 4a). By deconvolution[54,55] the trend becomes more evident; the ratios of the peak intensity and peak area (I_{ratio} and A_{ratio}, respectively) of the 3434 cm^{-1} (DA–OH) and 3226 cm^{-1} (DDAA–OH) bands increase as function of salt concentration (Table S3), indicating that the hydrogen-bonded "free" water relatively decreases (Figure 4b).

By their very compositions, the 1.9 m Na_2SO_4 and the hybrid electrolytes have H_2O/cation ratios of 14.6 and 9.0, respectively, which causes disruption of the hydrogen-bond water network. Furthermore, as the Walden plot (Figure 2) did indicate similar ionicities, the latter electrolyte should have less "free" water available and this might very well delay the onset of the oxidation and hence a wider ESW. Yet, we are far from seeing the same narrow feature at approximately 3550 cm^{-1} that emerges for WISEs at very high salt concentrations (>20 m) and correspond to H_2O/Na^+ ratios of 2–3.[56]

Electrochemical Characterisation

The electrochemical response in a CV of PTCDA with the 1 m Na_2SO_4 electrolyte shows a drastic decrease in current

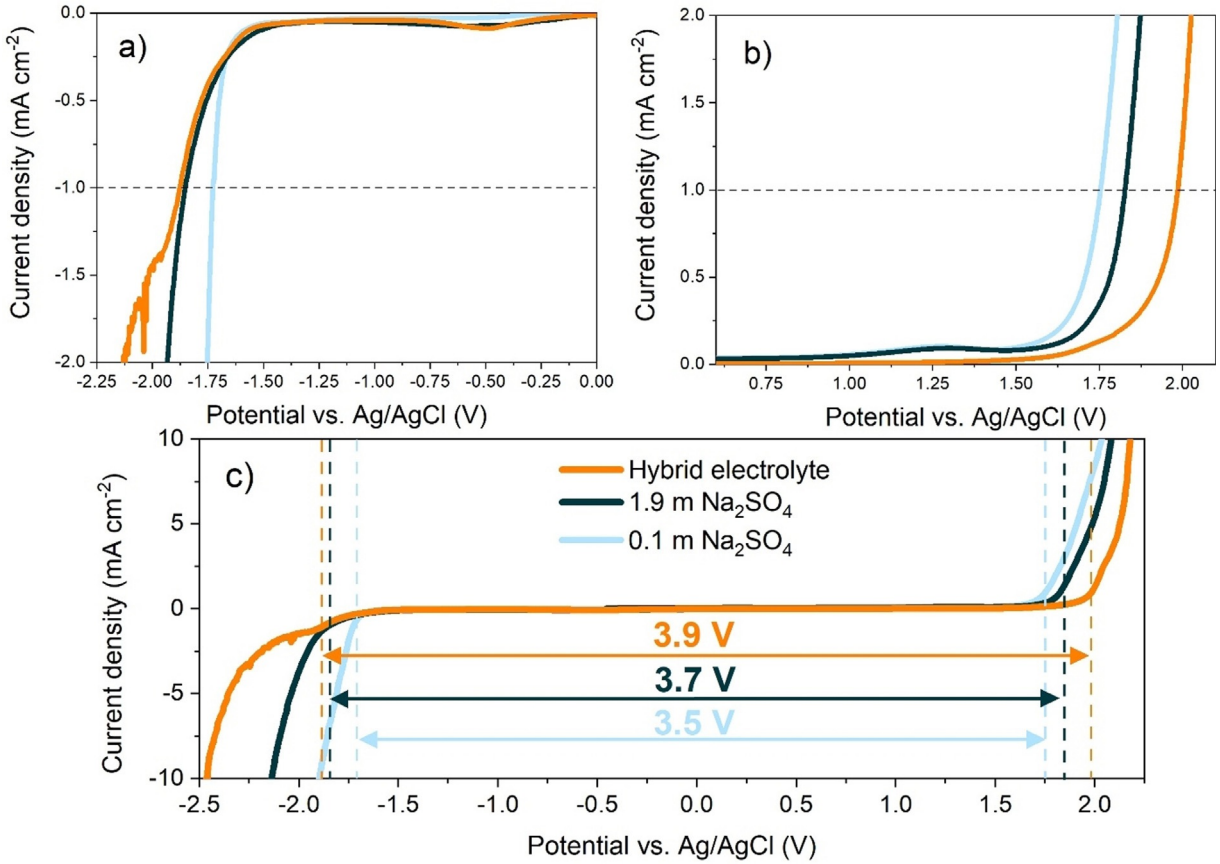

Figure 3. ESWs as obtained by LSV: a) the reduction part, b) the oxidation part, and c) the full window. Dashed lines in (a), (b) mark ± 1 mA cm^{-2}.

density already after 10 cycles (Figure 5 and Figure S2a), while together with the 1.9 m Na_2SO_4 electrolyte it vanished completely after only the very initial cycles (Figure S3a). This is attributed to the stability problems of the 1.9 m electrolyte towards saturation,[1] whereas the 1.6 m Na_2SO_4 electrolyte resulted in reversible and rather stable cycling (Figure S4a). Yet, fully reversible and much more stable cycling was obtained only for the hybrid electrolyte (Figure 5 and Figure S2b). The apparent difference is most easily ascribed to the reduced solubility of PTCDA by the lower water concentration, witnessed for WISEs[17] and discussed in more detail below, and in addition $MgSO_4$ might also improve the electrolyte stability during cycling.

At first, there is one redox peak during reduction, at ca. −0.7 V, and likewise one during oxidation, at ca. −0.4 V (Figure 5a). This is very similar to what has been observed for PTCDA using non-aqueous electrolytes, where also, after an electrochemical conditioning process during the initial cycle-(s)[17,28] that is, an activation phase, the peaks are split into several consecutive, stable, redox peaks. Here in aqueous media, the emerging peaks are shifted up in potential by ca. 30–100 mV (Figure 5b).

In contrast, for PTCDA in aqueous electrolytes with other cations, the CVs differ either in the number of peaks and/or in the redox potentials.[17,30,31] Thus, this strongly indicates that the primarily active cation in our electrolytes is Na^+.

Following the CVs, the GC charge/discharge profiles display extended voltage plateaus for the cells with the hybrid electrolyte vs. the other electrolytes (Figure 6). For the former, the initial discharge and charge capacities are 97 and 68 mAh g^{-1}, respectively, and after the first cycle it delivers a stable capacity of approximately 70 mAh g^{-1}, in excellent agreement with a two-electron reaction of PTCDA to Na_2PTCDA.[28] In stark contrast, most of the 1 m Na_2SO_4 electrolyte-based cells fail completely to cycle (Figure S5) and even if they do cycle (Figure 6a), there are severe problems already in the first cycle, likely due to PTCDA continuously being dissolved into the electrolyte.

Turning to the rate capability tests, again the 1 m Na_2SO_4 electrolyte-based cells have drastically impaired Coulombic efficiencies, especially at the lower C-rates (Figure 7a, different *y*-axis). Here the 1.6 m Na_2SO_4 electrolyte-based cells behave similarly (Figure S4b), however the cell with the 1.9 m Na_2SO_4 electrolyte failed to cycle (Figure S3b). In stark contrast, the hybrid electrolyte renders cells with Coulombic efficiencies close to 98% and an exceptional C-rate performance, despite its much higher viscosity (Figure 7d).

The cycling stability confirms the hybrid electrolyte to outperform the 1 m Na_2SO_4 electrolyte, the latter displaying neither reversible nor stable cycling (Figure 7bc). In contrast, the cells with the former display high Coulombic efficiencies (>94%) and capacity retention (98.7%, from the 2nd cycle)

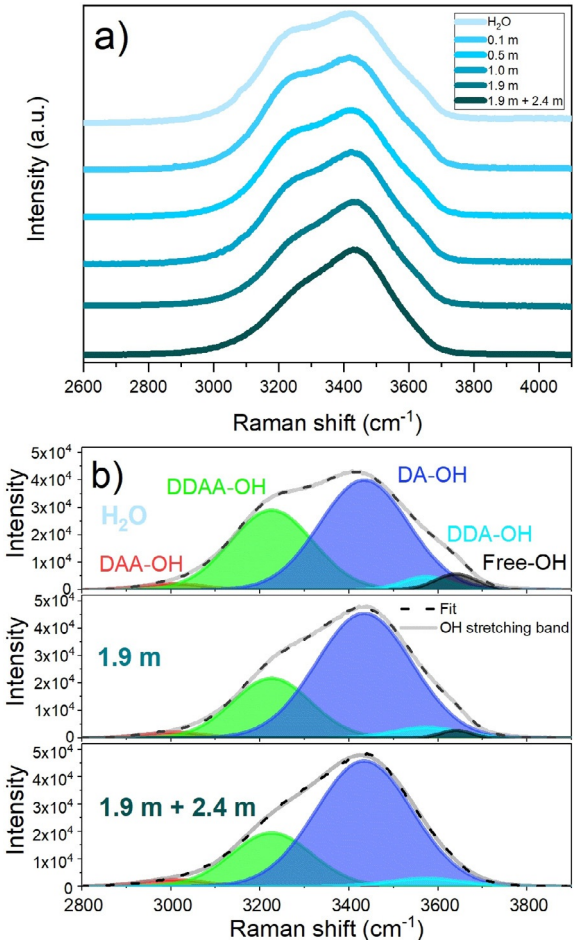

Figure 4. a) Raman spectra in the O–H stretching vibration region and b) the corresponding peak deconvolution of the pure water, the 1.9 m Na_2SO_4 electrolyte, and the hybrid electrolyte.

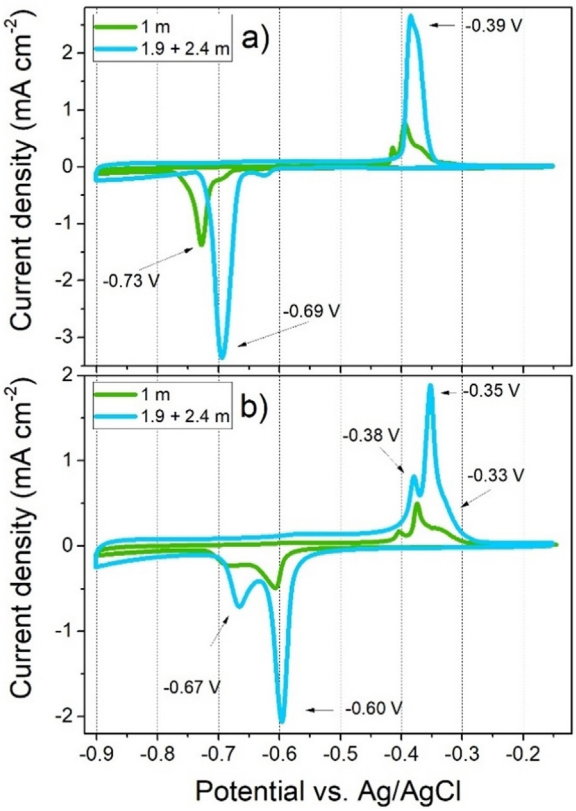

Figure 5. a) 1st and b) 10th CV cycle of PTCDA electrodes using the 1 m Na_2SO_4 and the hybrid electrolytes.

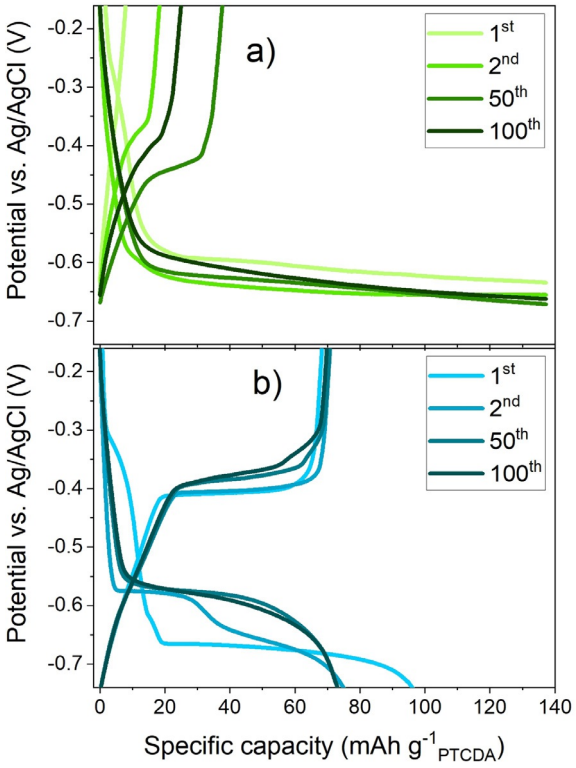

Figure 6. GC charge and discharge curves of PTCDA at 0.2 C using a) the 1 m Na_2SO_4 and b) the hybrid electrolyte.

(Figure 7 f), which at 1 C improves to >97% and 99.0% (Figure 7 e), respectively. In comparison, β-PTCDA with a 30 m KFSI WISE provided 82% capacity retention after 500 cycles at 2000 mA g^{-1} [17] (ca. 88–90% after 100 cycles by a rough eye-estimate), but even if this is for even longer cycling (×5) the significantly higher current density (×14) applied may hide/reduce parasitic reactions and contribute to the high stability.

To further investigate why the cells based on the hybrid electrolyte outperform all the others, the separators were recovered after 100 galvanostatic cycles. Indeed, there are no signs of any red colour indicating reduced[30,31] and dissolved PTCDA (Figure S6ab), quite unlike the situation for separators cycled in the 1 m Na_2SO_4 electrolyte (Figure S6cd) as well as, albeit much less so, the 1.6 m Na_2SO_4 electrolyte rate test cell (Figure S7). Furthermore, a discharged PTCDA electrode turns the water into a rich red colour upon immersion, and thus verifies the polarity increase of PTCDA when intercalated by cations (Figure S8). Moreover, and as previously reported,[17,30] $NaOH_{(aq)}$-immersed separators result in a green coloured solution from dissolved Na_2PTCDA as the structure is destroyed by OH^- (Figure S6e). Again, the separators from the cells cycled with the hybrid electrolyte remain colourless

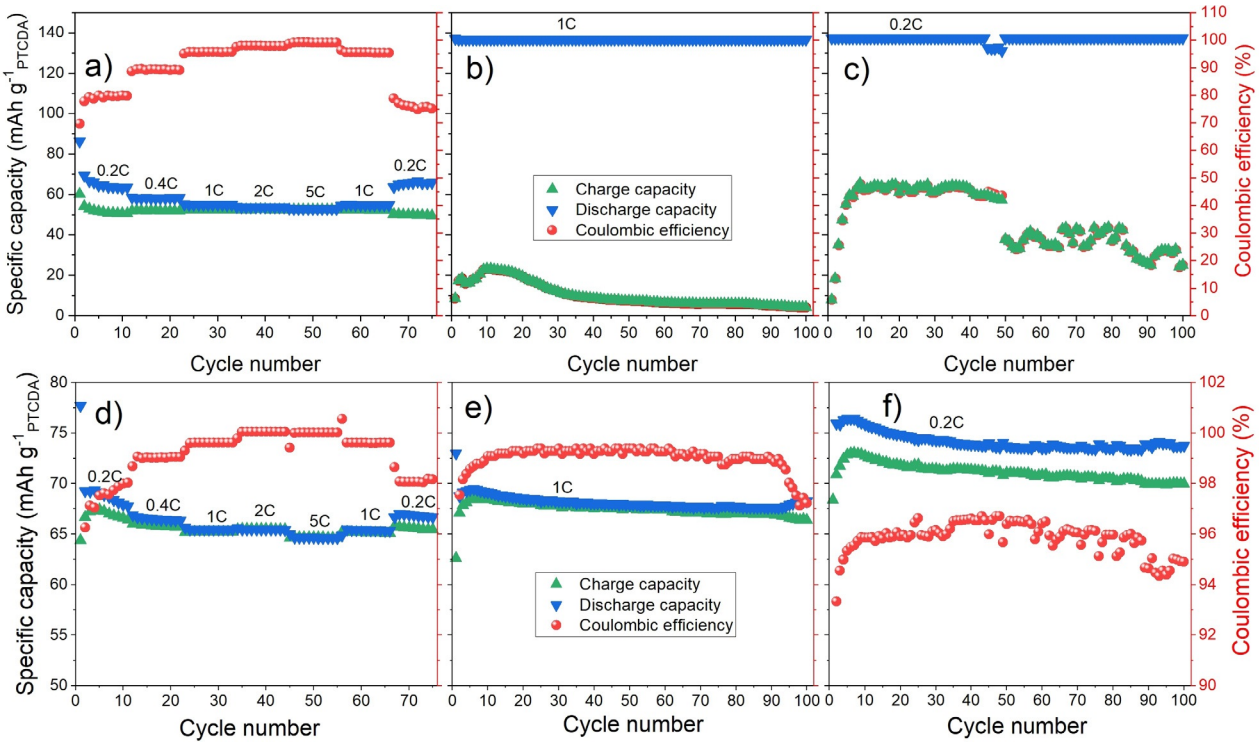

Figure 7. PTCDA electrode a,d) rate capability test and b,c,e,f) GC in a–c) 1 m Na_2SO_4 and d–f) the hybrid electrolyte. Note the right and left y-axis scale differences between (a)–(c) and (d)–(f).

(Figure S6e), confirming the suppressed dissolution of Na_2PTCDA.

Most likely the lower water concentration matters, but Yue et al. showed that also the dissolution kinetics are remarkably dependent on the viscosity,[57] which is very reasonable since the dissolved active material needs to be transported away as the electrode/electrolyte interface becomes saturated. We note that S. Li et al. also claim a protective $Mg(OH)_2$ interfacial layer to be formed during cycling using a 2.0 m Na_2SO_4 + 0.3 m $MgSO_4$ electrolyte and contribute to suppressing the dissolution of $NaTi_2(PO_4)_3$,[36] but again we are merely limited to their statement provided in the Abstract.

The energy efficiency, as noted by Eftekhari,[58] has been a neglected factor in battery research, and new materials exhibiting satisfactory Coulombic efficiencies, specific capacities, and (discharge) energy densities, still might lack sufficiently high energy efficiencies for practical development and commercialisation. As PTCDA displays a notable potential difference between the oxidation and the reduction (Figure 5), the energy efficiency of the electrode was calculated according to Equation (S4). By the 50th cycle, the electrode has an energy efficiency of 71% and 78% (Figure S9), calculated with respect to the AC CE and an imaginary cathode with constant voltage at 0.8 V vs. Ag/AgCl, respectively. This is on par with or slightly below typical LIB layered oxide cathodes,[59] where instead LIB anodes and supercapacitors tend to have lower energy efficiencies.[58] Therefore, PTCDA also in this regard is a promising active material choice for organic ASIBs.

Concluding Remarks

The herein presented hybrid electrolyte exhibits similar promising properties as WISEs, and at a drastically lowered materials price tag (Table S4), both in terms of physicochemical properties and more importantly by preventing PTCDA dissolution. The role of the additional salt, which seems not to be active electrochemically, is two-fold: the Raman spectra analysis indicates a decreased amount of "free water" which both extends the ESW and inhibits PTCDA dissolution during cycling, and the latter is also enforced by the higher viscosity than the conventional aqueous electrolytes. All this paves the way for more performant PTCDA-based ASIBs—both in terms of Coulombic efficiency, capacity retention, rate capability, and energy efficiency.

Acknowledgements

M.K., R.B., and P.J. would like to express their appreciation towards the Swedish Research Council for Sustainable Development (FORMAS) for enabling and supporting this work.

Conflict of Interest

The authors declare no conflict of interest.

Keywords: all-organic · anode · aqueous electrolyte · PTCDA · sodium-ion battery

[1] United Nations, "Goal 13. Take Urgent Action to Combat Climate Change and Its Impacts," can be found under https://www.un.org/sustainabledevelopment/climate-change/, **2015**.
[2] UN, Transforming Our World by 2030: A New Agenda For Global Action, **2015**.
[3] B. Dunn, H. Kamath, J. M. Tarascon, *Science* **2011**, *334*, 928 – 935.
[4] H. Pan, Y. S. Hu, L. Chen, *Energy Environ. Sci.* **2013**, *6*, 2338 – 2360.
[5] G. A. Blengini, C. E. L. Latunussa, U. Eynard, C. Torres de Matos, D. Wittmer, K. Georgitzikis, C. Pavel, S. Carrara, L. Mancini, M. Unguru, D. Blagoeva, F. Mathieux, D. Pennington, *Study on the EU's List of Critical Raw Materials (2020) Final Report*, Publications Office Of The European Union, **2020**.
[6] V. A. Oltean, S. Renault, M. Valvo, D. Brandell, *Materials* **2016**, *9*, 142.
[7] A. Bauer, J. Song, S. Vail, W. Pan, J. Barker, Y. Lu, *Adv. Energy Mater.* **2018**, *8*, 1702869.
[8] A. Ponrouch, R. Dedryvère, D. Monti, A. E. Demet, J. M. Ateba Mba, L. Croguennec, C. Masquelier, P. Johansson, M. R. Palacín, *Energy Environ. Sci.* **2013**, *6*, 2361 – 2369.
[9] D. Larcher, J. M. Tarascon, *Nat. Chem.* **2015**, *7*, 19 – 29.
[10] K. Kubota, S. Komaba, *J. Electrochem. Soc.* **2015**, *162*, A2538 – A2550.
[11] S. W. Kim, D. H. Seo, X. Ma, G. Ceder, K. Kang, *Adv. Energy Mater.* **2012**, *2*, 710 – 721.
[12] X. Dou, I. Hasa, D. Saurel, C. Vaalma, L. Wu, D. Buchholz, D. Bresser, S. Komaba, S. Passerini, *Mater. Today* **2019**, *23*, 87 – 104.
[13] X. Yin, S. Sarkar, S. Shi, Q. A. Huang, H. Zhao, L. Yan, Y. Zhao, J. Zhang, *Adv. Funct. Mater.* **2020**, *30*, 1908445.
[14] Y. Xu, M. Zhou, Y. Lei, *Mater. Today* **2018**, *21*, 60 – 78.
[15] Z. Song, H. Zhou, *Energy Environ. Sci.* **2013**, *6*, 2280 – 2301.
[16] W. Deng, Y. Shen, J. Qian, H. Yang, *Chem. Commun.* **2015**, *51*, 5097 – 5099.
[17] H. Chen, Z. Zhang, Z. Wei, G. Chen, X. Yang, C. Wang, F. Du, *Sustainable Energy Fuels* **2020**, *4*, 128 – 131.
[18] D. Pahari, S. Puravankara, *ACS Sustainable Chem. Eng.* **2020**, *8*, 10613 – 10625.
[19] S. Il Park, I. Gocheva, S. Okada, J. Yamaki, *J. Electrochem. Soc.* **2011**, *158*, A1067.
[20] K. Chayambuka, G. Mulder, D. L. Danilov, P. H. L. Notten, *Adv. Energy Mater.* **2018**, *8*, 1800079.
[21] J. Y. Luo, W. J. Cui, P. He, Y. Y. Xia, *Nat. Chem.* **2010**, *2*, 760 – 765.
[22] H. Long, W. Zeng, H. Wang, M. Qian, Y. Liang, Z. Wang, *Adv. Sci.* **2018**, *5*, 1700634.
[23] J. F. Whitacre, A. Tevar, S. Sharma, *Electrochem. Commun.* **2010**, *12*, 463 – 466.
[24] J. F. Whitacre, T. Wiley, S. Shanbhag, Y. Wenzhuo, A. Mohamed, S. E. Chun, E. Weber, D. Blackwood, E. Lynch-Bell, J. Gulakowski, C. Smith, D. Humphreys, *J. Power Sources* **2012**, *213*, 255 – 264.
[25] W. Deng, Y. Shen, J. Qian, H. Yang, *Chem. Commun.* **2015**, *51*, 5097 – 5099.
[26] T. Gu, M. Zhou, M. Liu, K. Wang, S. Cheng, K. Jiang, *RSC Adv.* **2016**, *6*, 53319 – 53323.
[27] X. Han, C. Chang, L. Yuan, T. Sun, J. Sun, *Adv. Mater.* **2007**, *19*, 1616 – 1621.
[28] W. Luo, M. Allen, V. Raju, X. Ji, *Adv. Energy Mater.* **2014**, *4*, 1400554.
[29] M. Möbus, N. Karl, T. Kobayashi, *J. Cryst. Growth* **1992**, *116*, 495 – 504.
[30] X. Wang, C. Bommier, Z. Jian, Z. Li, R. S. Chandrabose, I. A. Rodríguez-Pérez, P. A. Greaney, X. Ji, *Angew. Chem. Int. Ed.* **2017**, *56*, 2909 – 2913; *Angew. Chem.* **2017**, *129*, 2955 – 2959.
[31] I. A. Rodríguez-Pérez, Y. Yuan, C. Bommier, X. Wang, L. Ma, D. P. Leonard, M. M. Lerner, R. G. Carter, T. Wu, P. A. Greaney, J. Lu, X. Ji, *J. Am. Chem. Soc.* **2017**, *139*, 13031 – 13037.
[32] L. Jiang, Y. Lu, C. Zhao, L. Liu, J. Zhang, Q. Zhang, X. Shen, J. Zhao, X. Yu, H. Li, X. Huang, L. Chen, Y. S. Hu, *Nat. Energy* **2019**, *4*, 495 – 503.
[33] L. Jiang, L. Liu, J. Yue, Q. Zhang, A. Zhou, O. Borodin, L. Suo, H. Li, L. Chen, K. Xu, Y. Hu, *Adv. Mater.* **2020**, *32*, 1904427.
[34] K. Xu, *Chem. Rev.* **2004**, *104*, 4303 – 4417.
[35] L. J. Vimmerstedt, S. Ring, C. J. Hammel, *Current Status of Environmental, Health, and Safety Issues of Lithium Ion Electric Vehicle Batteries*, Golden, CO, **1995**.
[36] S. Li, Z. Cao, W. Wang, X. Zhang, X. Xiang, *J. Electrochem.* **2021**, *0*, 211.
[37] D. Reber, R. Figi, R. S. Kühnel, C. Battaglia, *Electrochim. Acta* **2019**, *321*, 134644.
[38] D. Reber, R. S. Kühnel, C. Battaglia, *Sustainable Energy Fuels* **2017**, *1*, 2155 – 2161.
[39] R. S. Kühnel, D. Reber, C. Battaglia, *ACS Energy Lett.* **2017**, *2*, 2005 – 2006.
[40] J. Yin, C. Zheng, L. Qi, H. Wang, *J. Power Sources* **2011**, *196*, 4080 – 4087.
[41] G. Tammann, W. Hesse, *Z. Anorg. Allg. Chem.* **1926**, *156*, 245 – 257.
[42] G. S. Fulcher, *J. Am. Ceram. Soc.* **1925**, *8*, 789 – 794.
[43] P. L. Stigliano, N. Pianta, S. Bonizzoni, M. Mauri, R. Simonutti, R. Lorenzi, B. Vigani, V. Berbenni, S. Rossi, P. Mustarelli, R. Ruffo, *Phys. Chem. Chem. Phys.* **2021**, *23*, 1139 – 1145.
[44] M. S. Ding, A. Von Cresce, K. Xu, *J. Phys. Chem. C* **2017**, *121*, 2149 – 2153.
[45] P. Walden, *Z. Phys. Chem.* **1906**, *55*, 207 – 246.
[46] M. B. Herath, S. E. Creager, A. Kitaygorodskiy, D. D. DesMarteau, *ChemPhysChem* **2010**, *11*, 2871 – 2878.
[47] A. Dave, K. L. Gering, J. M. Mitchell, J. Whitacre, V. Viswanathan, *J. Electrochem. Soc.* **2020**, *167*, 013514.
[48] Q. Zheng, S. Miura, K. Miyazaki, S. Ko, E. Watanabe, M. Okoshi, C. Chou, Y. Nishimura, H. Nakai, T. Kamiya, T. Honda, J. Akikusa, Y. Yamada, A. Yamada, *Angew. Chem. Int. Ed.* **2019**, *58*, 14202 – 14207; *Angew. Chem.* **2019**, *131*, 14340 – 14345.
[49] M. Hilder, M. Gras, C. R. Pope, M. Kar, D. R. Macfarlane, M. Forsyth, L. A. O'Dell, *Phys. Chem. Chem. Phys.* **2017**, *19*, 17461 – 17468.
[50] M. Mclin, C. A. Angelí, *Contrasting Conductance/Viscosity Relations in Liquid States of Vitreous and Polymer "Solid" Electrolytes*, **1988**.
[51] J. Han, M. Zarrabeitia, A. Mariani, Z. Jusys, M. Hekmatfar, H. Zhang, D. Geiger, U. Kaiser, R. J. Behm, A. Varzi, S. Passerini, *Nano Energy* **2020**, *77*, 105176.
[52] L. Niu, L. Chen, J. Zhang, P. Jiang, Z. Liu, *J. Power Sources* **2018**, *380*, 135 – 141.
[53] J. D. Benck, B. A. Pinaud, Y. Gorlin, T. F. Jaramillo, *PLoS One* **2014**, *9*, e107942.
[54] Q. Sun, *Vib. Spectrosc.* **2009**, *51*, 213 – 217.
[55] Y. Ma, W. Yan, Q. Sun, X. Liu, *Geosci. Front.* **2021**, *12*, 1018 – 1030.
[56] M. H. Lee, S. J. Kim, D. Chang, J. Kim, S. Moon, K. Oh, K. Y. Park, W. M. Seong, H. Park, G. Kwon, B. Lee, K. Kang, *Mater. Today* **2019**, *29*, 26 – 36.
[57] J. Yue, L. Lin, L. Jiang, Q. Zhang, Y. Tong, L. Suo, Y. Hu, H. Li, X. Huang, L. Chen, *Adv. Energy Mater.* **2020**, *10*, 2000665.
[58] A. Eftekhari, *Sustainable Energy Fuels* **2017**, *1*, 2053 – 2060.
[59] J. Kasnatscheew, M. Evertz, R. Kloepsch, B. Streipert, R. Wagner, I. Cekic Laskovic, M. Winter, *Energy Technol.* **2017**, *5*, 1670 – 1679.

Manuscript received: August 27, 2021
Accepted manuscript online: September 16, 2021
Version of record online: October 12, 2021

